Kinetic plasma chemistry model of pulsed transient spark discharge in air coupled with nanosecond time-resolved imaging and spectroscopy.

Mário Janda, Karol Hensel, and Zdenko Machala

Division of Environmental Physics, Faculty of Mathematics, Physics and Informatics, Comenius University, Mlynská dolina F2, 842 48 Bratislava, Slovakia

janda@fmph.uniba.sk

Abstract

Based on experimental results, Transient Spark (TS) discharge in atmospheric air is an efficient source of NO_x for biomedical applications with a negligible O_3 production. The TS discharge is characteristic by short (~10 ns) high current (~A) pulses initiated by streamer. The time-resolved optical imaging and spectroscopy of the TS discharge revealed that the primary streamer (ionization wave) is followed by the secondary streamer and enabled us to reconstruct the temporal evolution of the reduced electric field strength *E/N(t)*. This was then used for chemical kinetic model of the primary and the secondary streamer phases of the TS discharge. In this chemical kinetic modeling we focus on the generation of selected reactive oxygen and nitrogen species (RONS) with antibacterial and other biological effects: O, N, NO, NO_2, and O_3. We proved that the secondary streamer plays more important role in the induced chemistry than the primary streamer. In the simulation with the secondary streamer, the densities of RONS were increased by an order of magnitude if compared to the simulation without the secondary streamer, despite the same peak electron densities. The dominant intermediate product of the secondary streamer chemistry is atomic oxygen. Without the spark phase, this would lead to the generation of ozone as the dominant final product, however, in the spark pulse phase following the streamer(s), the chemistry is twisted towards dominant production of NO_x.

1. Introduction

The transient spark (TS) is a dc-operated, self-pulsing and filamentary discharge with typical repetition frequency in the range 1-10 kHz. Fundamental research of the positive polarity TS revealed that it is characteristic by the short (~10-100 ns) spark current pulses, having maximum amplitude in the range of a few Amps [1]. Thanks to the short spark pulse duration and limited amount of deposited energy (~1 mJ/pulse), significant heating of the treated gas is avoided and the generated plasma is non-equilibrium and highly reactive, with an electron density above 10^{17} cm^{-3} [2]. Its chemical activity is comparable with nanosecond repetitively pulsed (NRP) spark discharges [3]. The advantage of TS is no need of special and expensive high voltage pulsers with high repetitive frequencies and nanosecond rise-times typically used to generate NRP discharges [4-6].

The reactive plasma properties predetermine the TS for environmental and biomedical applications or generation of nanoparticles [3, 7, 8]. In biomedical applications, the emerging fundamental research is focused to assess the roles of various plasma agents (e.g. UV radiation, electric field, reactive neutral and charged particles). At present, the major antibacterial role in atmospheric pressure plasmas generated in air is typically attributed to reactive oxygen and nitrogen species (RONS) [9, 10]. Besides the antimicrobial effects, the RONS also play a significant role in cancer therapies. Water and aqueous media activated by plasma containing RONS can induce cancer cell apoptosis by facilitating an accumulation of intracellular RONS [11]. Although further details on the exact interaction pathways of RONS with cancer cells is still needed, it was shown that reactive oxygen species can induce cancer cells death by impairing the function of intracellular regulatory factors [12].

Depending on the used electrical discharge, different gaseous RONS can dominate in the treated gas. For example, the O_3 generation is very efficient by cold plasma sources, such as dielectric barrier or streamer corona discharges [13-15]. Various plasma sources can also generate significant amounts of NO_x [16-19]. The antibacterial potential of NO_2 is known [20, 21], and has been already commercially introduced [22], but new types of discharges optimized for bio-medical plasma applications are still being developed and studied. Several recent papers report investigating the NO_x formation and their bactericidal effects in a hybrid glow-spark discharges or in dielectric barrier discharges in air [23–25]. We recently reported the efficient generation of NO_x by TS discharge [26]. The NO_x production rate ~$7x10^{16}$ molecules/J was achieved. The NO_2/NO ratio decreased with increasing TS repetition

frequency, which was attributed to the complex frequency-dependent discharge properties and thus changing NO_2/NO generating mechanisms. We therefore decided to use kinetic modeling to better understand the dominant mechanisms of NO_x and other RONS (e.g. O, N, O_3) generation in the TS discharge.

The modeling of chemical kinetics aiming to calculate the density evolution of all species included in the kinetic model is an effective tool for complex systems description. In many cases, it is the most powerful way to solve problems where the complexity inhibits using analytical methods and direct experimental measurements. It is commonly used not only for the modeling of cold plasma chemistry including RONS generation in atmospheric pressure plasma jets [27, 28], but also for the description of high-temperature steady-state arc plasmas [29], nanosecond duration of streamer propagation [30], and other problems in plasma physics and chemistry.

The chemical kinetic modeling could also help us to improve our understanding of the TS discharge evolution, the transition from streamer to gas breakdown and spark formation. The individual phases of the TS discharge were identified by optical diagnostic techniques [31, 32]. The results enabled the visualization of different phases of the TS development including the primary streamer, the secondary streamer, and the transition to the spark.

The primary streamer (ionization wave) has been previously identified in the TS based on oscilloscopic current measurements [1]. Thanks to the space charge, the electric field in the primary streamer's head can reach more than 200 kV cm^{-1} [33, 34], so the chemical and ionization processes are very efficient there. Streamers are thus considered to be crucial for the efficiency of plasma-induced chemistry at atmospheric pressure. On the other side, Marode et al. [35] stressed out the importance of the secondary streamer on plasma induced chemistry in prevented spark discharge. The name 'secondary streamer' was first used by Loeb who suggested it was a new ionization wave [36], although according to Bastien and Marode, it is governed by attachment processes [37]; more precisely, by the distribution of the attachment rate along the plasma filament generated by the primary streamer. Higher attachment rate leads to the faster decrease of the electron density. This is equivalent to the decrease of the plasma conductivity and results in the reduced electric field *E/N* increase near the anode [35, 37-39]. The *E/N* near the anode can be as high as ~80 Td [35]. This is high enough for the generation of excited N_2 species emitting photons, observed as 'the secondary streamer'.

The objective of this paper is to present a chemical kinetic model developed for TS discharge. More specifically, the model describing the primary and secondary phases of the TS that precede the formation of the spark. This model can be used to determine the evolution of densities of species that are not measurable via available experimental techniques. Here we focus on selected RONS: O, N, O_3, NO, and NO_2. Compared to the previous version of our model presented in Ref. [40], the presented model includes more species, more reactions and besides the primary streamer, we also included the secondary streamer phase. The validity of the model was tested by comparing the calculated electron and $N_2(C)$ densities with experimental data [1, 2, 32, 41].

2. Transient Spark

TS is a dc-driven self-pulsing discharge with periodic streamer-to-spark transition with a repetition frequency of 1-10 kHz. Figure 1 shows a schematic of the electric circuit used to generate the positive TS discharge by a positive polarity dc high-voltage (HV) power supply connected to a metal needle HV electrode via a series resistor (R = 5-10 MΩ). In the same way, the negative TS can be generated using negative dc HV power supply [42]. The typical distance d between the tip of the HV electrode and a grounded planar electrode is 4-10 mm.

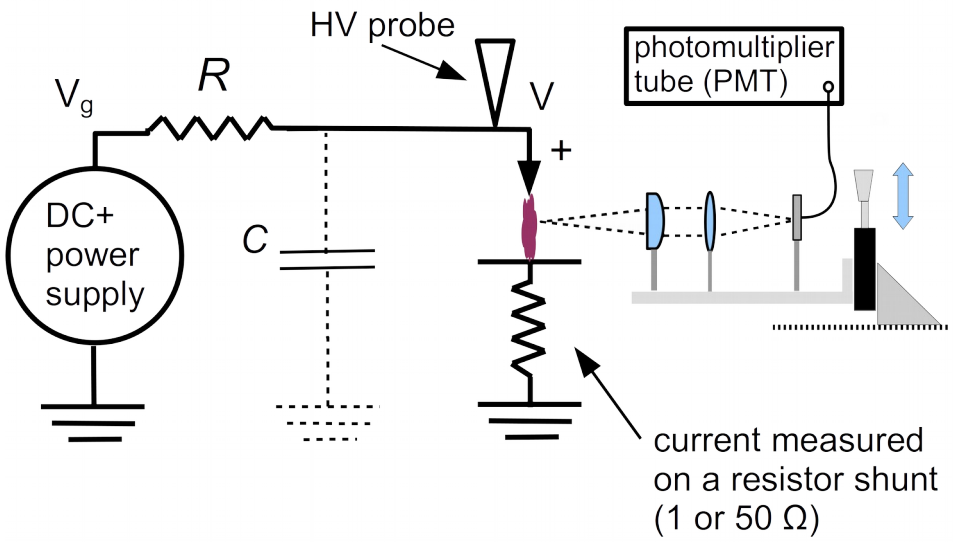

Fig. 1. Schematic of the setup used for generation and diagnostics of the positive transient spark (TS).

The measurement of electric characteristics showed that the positive TS is initiated by a current pulse with typical amplitude 50-100 mA (phase A in Fig. 2), appearing when the potential on the stressed electrode reaches the voltage V_{TS} characteristic for the TS discharge. This initial current pulse was attributed to a streamer [1]. The optical visualization of the TS evolution revealed its more complex behavior during the discharge initiation phase [31, 32]. In our previous work [32], streak camera-like images were obtained using spatio-temporal reconstruction of the discharge emission detected by a photomultiplier tube with light collection system placed on a micrometric translation stage (Fig. 1). In order to isolate the N_2 (C–B, 0–0) transition for the PMT measurements, a bandpass interference filter was inserted into the optical path. The recorded temporal evolution of the TS shows two subsequent luminous events identified as the primary streamer (ionization wave), followed by the secondary streamer (A1 and A2, respectively, in Fig. 3).

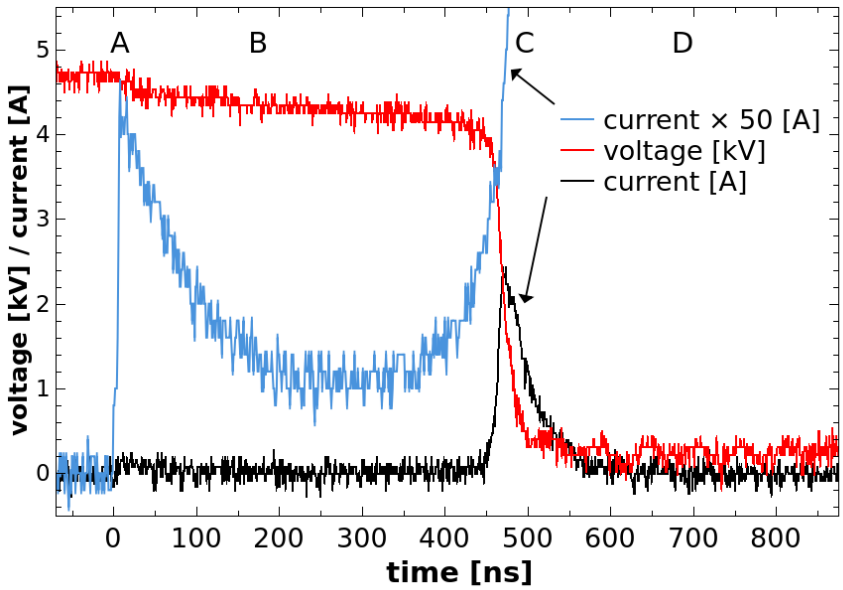

Fig. 2. Typical voltage and current waveforms of the TS, gap $d \approx 4.5$ mm, $C \approx 24$ pF, $R = 6.5$ MΩ, $f \approx$ 3.5 kHz.

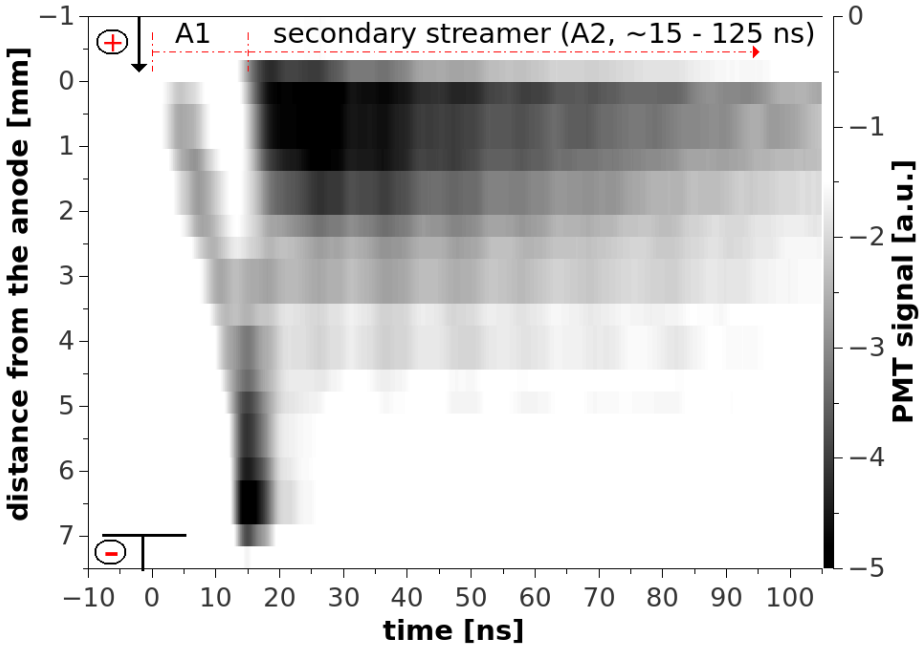

Fig. 3. Visualization of the primary and secondary streamer from spatio-temporal reconstruction of the PMT signals, filtered emission from N_2 (C–B, 0–0) transition, $f \approx 2$ kHz, $d = 7$ mm.

The primary streamer propagates through the whole gap at any TS repetition frequency, but the behavior of the secondary streamer changes as the TS repetition frequency increases [32]. If the frequency is approximately 3 kHz or higher, the secondary streamer propagates through the whole gap and it is relatively quickly followed by the spark formation, because the entire streamer-to-spark transition delay time τ is short and decreases down to ~100 ns at ~6 kHz [41]. In this work we focus on lower f (< 3 kHz), where the secondary streamer does not propagate through the whole gap and the average streamer-to-spark transition delay time τ (phase B in Fig. 2) is much longer. It varies from a few hundred ns up to several μs [41]. The emission from the N_2 (C-B) transition (2^{nd} positive system) representing the secondary streamer disappears long before transition to the spark (Fig. 4). This enables us to focus on the secondary streamer phase without considering additional issues related to the spark formation.

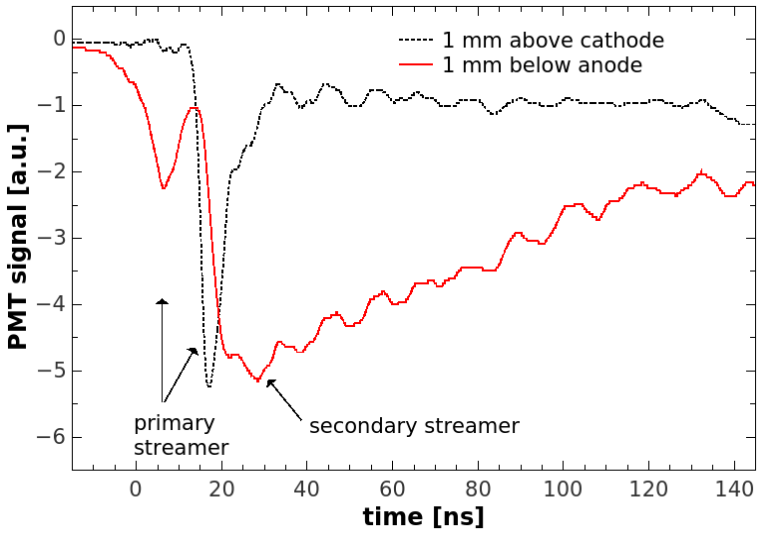

Fig. 4. PMT signals of the TS discharge (streamer phase), emission from N_2 (C–B, 0–0) transition, measured near the anode and the cathode, respectively, $f \approx 2$ kHz, $d = 7$ mm.

During the spark phase, the discharge current reaches a high value (~1-10 A) for a short time and the voltage drops to almost zero (phase D in Fig. 2). This current pulse is due to the discharging of the capacity C, given mainly by the intrinsic capacity of the HV cable connecting the ballast resistor R and the anode and also including the internal capacity of the discharge chamber and the capacity of the HV probe. At least ~10 pF is needed to achieve ~1 A current pulses. With typical $C \approx 30$ pF, the pulses can exceed 10 A, but the amount of energy in a single TS pulse is still quite low (~1 mJ). Thus, the generated plasma cannot reach thermal equilibrium, the discharging is very fast (~10-100 ns) and the discharge current quickly drops to much lower value (~1 mA). This is due to the ballast resistor R that limits the current delivered to the plasma by the used dc power supply. As a result, the plasma starts to decay after the spark pulse (phase D in Fig. 2). Eventually, the plasma resistance exceeds R and the potential V on the stressed electrode gradually increases as the capacitor C recharges. A new TS pulse, initiated by a new primary streamer, occurs when V reaches again the characteristic voltage V_{TS}. The TS discharge is thus based on repetitive charging and discharging of C. With the known V_g and R, the value of C can be estimated from the measured repetition frequency f of this process according to the formula derived in Ref. [1]:

$$f = \left[RC \ln\left(\frac{V_g}{V_g - V_{TS}} \right) \right]^{-1}. \qquad (1)$$

3. Model Description

The density evolution of all species in a kinetic model can be derived from the used reaction set

$$\frac{dN_i}{dt} = S_i = \sum_{j=1}^{j=n} S_{ij} \tag{2}$$

Here, S_i is a total production term for species X_i, while S_{ij} is a production term for species X_i in a specific reaction j. Next, n is the total number of reactions, and N_i is the number density of species X_i. For the calculation of S_{ij}, the stoichiometric coefficients (lower case letters) of the X_i species in the j^{th} reaction

$$aX_i + bX_{i+1} + \ldots = a'X_i + b'X_{i+1} + \ldots \tag{3}$$

must be taken into the account

$$S_{ij} = (a - a') \times R_j . \tag{4}$$

The term R_j is the rate of the j^{th} chemical reaction

$$R_j = k_j \times \prod_{m=i}^{m=i+l} N_m^{\alpha_m} \tag{5}$$

,

where k_j is the reaction rate coefficient (rate constant), l is the total number of species involved in the j^{th} reaction, N_m is the actual density of the m^{th} species, and α_m is the partial order of reaction with respect to the species m.

In practice, it is necessary to solve this set of reactions numerically, using a solver of differential equations. We based our model on the existing ZDPlasKin module [43] that includes a Fortran 90 version of the VODE solver for numerical solution of system of ordinary differential equations [44], using Adams' or backward differentiation formula methods. Authors of ZDPlasKin also provide a ready-to-use list of plasmachemical processes in nitrogen-oxygen mixtures with all necessary rate coefficients [45], based on reactions listed in Ref. [46] and [47]. We used this set of reactions (version 1.03) in our simulations too. It is a set of about 650 chemical reactions among 53 species, namely, molecules N_2 (X^1, v = 0-8), N_2 (A^3, B^3, a'^1, C^3), O_2 (X^3, v = 0-4), O_2 (a^1, b^1, 4.5 eV), O_3, NO, N_2O, NO_2, NO_3 and N_2O_5, atoms N (^4S, ^2D, ^2P) and O (^3P, ^1D, ^1S), positive ions N^+, N_2^+, N_3^+, N_4^+, O^+, O_2^+, O_4^+, NO^+, N_2O^+, NO_2^+ and $O_2^+N_2$, negative ions O^-, O_2^-, O_3^-, O_4^-, NO^-, N_2O^-, NO_2^- and NO_3^-, and electrons. The electron impact excitation of other electronic states of nitrogen is also included, but the

model assumes their instantaneous relaxation: $N_2(W^3, B'^3) \rightarrow N_2(B^3)$; $N_2(a^1, w^1) \rightarrow N_2(a'^1)$, and $N_2(E^3, a''^1) \rightarrow N_2(C^3)$. The generalized level O_2(4.5 eV) corresponds to $O_2(A^3, C^3)$ and $O_2(c^1)$ states.

The rate constants of reactions between heavy species from this list are calculated from the thermodynamic gas temperature T_g. This temperature is frequently assumed to be equal for all ions and neutrals even in non-thermal plasmas. This is no longer valid for electrons. Their energy is usually much higher, as well as their temperature (T_e). The rate constant for electron impact reactions must be calculated from electron energy distribution function (EEDF). The EEDF is usually obtained by solving the Boltzmann equation for free electrons. The ZDplasKin package includes a Bolsig+ solver for the numerical solution of the Boltzmann equation. The principle and characteristics of Bolsig+ solver are described in more detail in [48]. A set of required electron scattering cross sections was taken from the LXCat project database [49]. Namely, we used the databases found in [50, 51] (N_2, and O_2), in [52] (N_2 (A^3, a'^1), $O_2(a^1, b^1)$, O_3, O, O^- and N), in [53] (NO, N_2O), and in [54] (NO_2). Besides the collisions with heavy particles, the Bolsig+ solver also handles the electron-electron interactions if the degree of ionization exceeds selected threshold, the default value is 10^{-5}.

4. Results and Discussion

The TS discharge evolution, as described in Section 2, is composed of several consecutive phases. Each phase is characterized by different time scales and different dominant processes. Here we focus on the relatively short (<250 ns) initial phase of the TS discharge consisting of the primary and the secondary streamer. These phases of the TS are characterized by fast changes of E/N and T_e. It is therefore necessary to determine the density of many species that could influence the plasma induced chemistry with good temporal resolution (~ns), while processes such as diffusion can be neglected on this short time scale.

4.1. Primary streamer simulation

The primary streamer is an ionization wave propagating from the HV electrode towards the grounded electrode. The modeling of primary streamer propagation requires at least 2-D model using axisymmetry assumption [55]. The 0-D kinetic model calculates densities of many species in a single point in space and obviously cannot be used to simulate propagation of the ionization wave. The

influence of the primary streamer on the rates of chemical reactions in the 0-D kinetic model can be introduced by using appropriate temporal evolution of *E/N*, based on the extensively published primary streamer characteristics [33, 34, 55-59] and our experimental results [31].

We defined the temporal evolution of *E/N* in a selected point *H*, where the primary streamer's head with the peak reduced electric field strength E/N_{max} [Td] appears at time t_H, by the following formula:

$$E/N(t)=\begin{cases} E/N_{before}+\dfrac{(E/N_{max}-E/N_{before})\,l_t}{t_H-t+l_t}, & t<t_H, \\ E/N_{after}+(E/N_{max}-E/N_{after})\exp(-2\,l_t(t-t_H)), & t>t_H. \end{cases} \quad (6)$$

This formula is based on work of Kulikovsky [34] and Naidis [58], describing the axial distribution of the electric field strength during the primary streamer propagation. Equation (6) well describes a gradual increase of *E/N* in the point H when $t<t_H$, from the initial value E/N_{before} towards the peak value E/N_{max}. The rate of this increase is given by the parameter l_t [ns]. When $t>t_H$, equation (6) gives a sharp decrease of E/N_{max} to much lower value E/N_{after} characteristic for the relatively conductive plasma channel generated behind the primary streamer's head. This *E/N(t)* profile is in agreement with temporal evolution of *E* during the streamer propagation calculated by Bonaventura et al. [59].

Table 1 shows the values of the parameters from Eq. (6) that we used in our simulations. Table 1 contains also another input parameters influencing calculated densities of species in our simulations, such as initial electron density $n_e(0)$, initial gas temperature $T_g(0)$, or initial molar fraction of NO and NO_2, χ_{NO} or χ_{NO2}, respectively. Values of all these parameters were selected based on our previous experimental studies, and values found in the literature. More details can be found in Appendix 1.

We varied the values of these parameters in order to achieve the peak electron density during the primary streamer close to the experimentally observed $n_e \approx 10^{14}$ cm^{-3} [2]. As Fig. 5 shows, the same peak electron density can be achieved by various combinations of parameters in Table 1. However, we observed that within ranges given in Table 1, the evolution of $n_e(t)$, RONS and $N_2(C^3\Pi)$ densities after the primary streamer were not significantly influenced by the selection of the initial values of these parameters (Fig. 5).

From the simulations of the primary streamer we also concluded that when *E/N* is above ~100 Td and $N_2(C)$ species are effectively produced by electron impact excitation collisions, the peak density of $N_2(C)$ is always close to n_e. This results from the fact that the electron impact excitation collisions are the key source of $N_2(C)$ in this case [60].

parameter	tested range	values used in the final calculations	
		$n_e = 10^{14}$ cm^{-3} reached during the primary streamer	$n_e = 10^{14}$ cm^{-3} reached during the secondary streamer
E/N_{before} [Td]	40 - 125	100	100
E/N_{max} [Td]	200 - 350	306	292
E/N_{after} [Td]	40 - 70	40	40
t_H [ns]	20 - 40	30	30
l_t [ns]	1 - 3	2	2
$n_e(0)$ [cm^{-3}]	10^3 - 10^{10}	10^8	10^8
χ_{NO} and χ_{NO2}	0 - 10^{-4}	10^{-5}	10^{-5}
$T_g(0)$ [K]	300 - 350	350	350

Table 1 – Input parameters and their values used for simulation of the primary streamer.

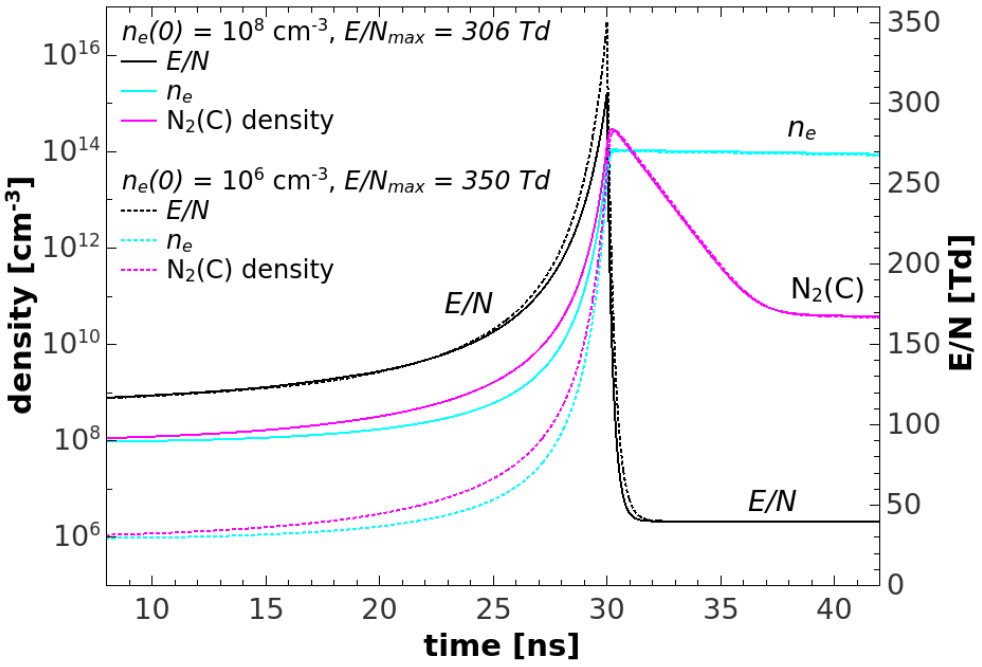

Fig. 5 – Example of the used *E/N* profiles describing the primary streamer with calculated densities of electrons and $N_2(C)$ species, E/N_{max} = 306 and 350 Td, $n_e(0)$ = 10^8 cm^{-3} and 10^6 cm^{-3}, respectively. Other input parameters are described in Table 1, column 3.

Behind the streamer's head, the electric field is too weak and electrons do not have enough energy to generate sufficient amount of $N_2(C)$ species and their density drops quickly. Quenching reaction

$$N_2(C) + O_2 \rightarrow N_2 + O + O(^1S) \qquad (7)$$

represents the major sink of $N_2(C)$ states, contributing to the production of atomic oxygen (O). There are several other important O generation pathways, and the O density in post primary streamer period increased up to almost 10^{16} cm^{-3} in our simulations (Fig 6). The efficiency of atomic nitrogen (N) production is much lower and the maximum N density slightly exceeded 10^{14} cm^{-3} only. However, both atomic species (O and N)) are intermediate products and they disappear at longer time scale (Fig. 6), while stable products like O_3, NO and NO_2 are generated. Fig. 6 shows results from the long time scale simulation with constant E/N = 40 Td and constant gas temperature T_g = 350 K after the primary streamer, without the secondary streamer phase and without the spark phase. Under these conditions, the final ozone density significantly exceeds the densities of nitrogen oxides. This is in opposite to the TS discharge time-integrated (over all TS phases) species production, where we experimentally measured high densities of NO and NO_2, while the concentration of produced O_3 was negligible [26]. For this reason we suppose that the chemistry induced by TS is not determined by the primary streamer, but more importantly by the following secondary streamer and spark phases.

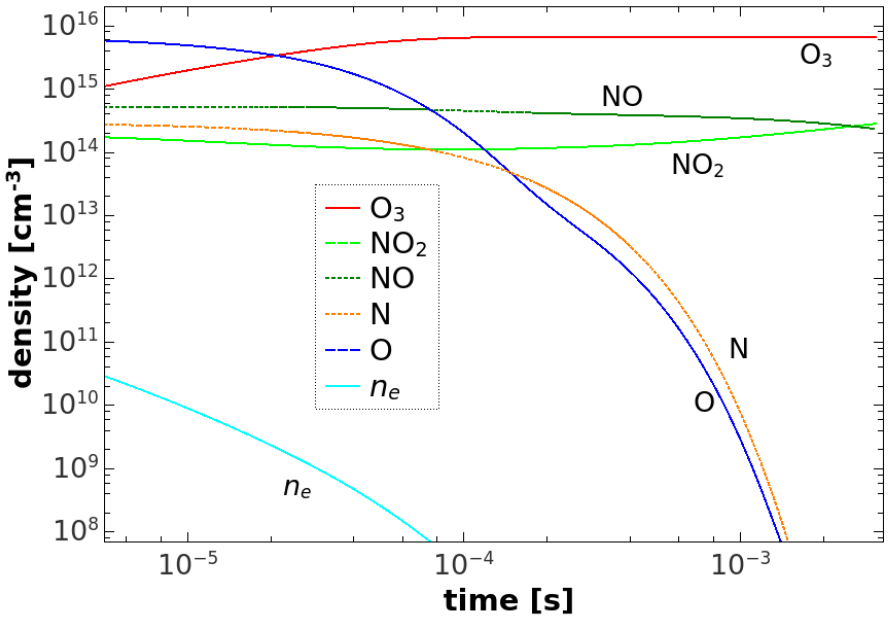

Fig. 6 - Calculated densities of electrons and selected RONS, input parameters set as in Table 1, column 3, constant T_g and E/N after the primary streamer without secondary streamer and spark.

4.2 Secondary streamer modeling

The average axial E/N_{avg} in the plasma channel created by the primary streamer in TS was estimated to be around 60-70 Td, assuming homogeneous axial E/N distribution [41]. In fact, the assumption of

homogeneous axial *E/N* is not quite correct and the appearance of the secondary streamer near the anode (Figure 3, time around 20 ns) indicates *E/N* enhancement in this region, where *E/N* can reach value above 80 Td [35].

parameter	**value**
primary to secondary streamer delay	20 ns
secondary streamer *E/N* rise time	1 ns
maximum *E/N* during the secondary streamer E/N_{sec_max}	60 – 135 Td
duration of constant E/N_{sec_max}	10 ns
duration of linear *E/N* decrease from peak to average value	65 ns

Table 2 – Secondary streamer parameters used in presented model.

We simulated the *E/N(t)* profile in the point 1 mm below the tip of the anode. The appearance of the secondary streamer in the moment when the primary streamer reaches the cathode is represented by a fast increase of *E/N* (we used characteristic rise time 1 ns) from the value right after the primary streamer head (E/N_{after}) to the secondary streamer peak value (E/N_{sec_max}). Based on our experimental data (Fig. 3), the 20 ns delay between the appearance of the primary and the secondary streamer 1 mm below the anode was used. Eventually, the emission related to the secondary streamer disappears. This can be interpreted as smoothening of the axial *E/N* profile towards a homogeneous distribution with $E/N(t,x) = E/N_{avg}$. Based on the experimental data (Fig. 4), we estimated the duration of the secondary streamer to 75 ns, with 10 ns plateau (constant $E/N(t) = E/N_{sec\_max}$) followed by linear decrease of *E/N* from E/N_{sec_max} to E/N_{avg} = 60 Td during 65 ns (Fig. 7). Characteristics of the *E/N* temporal evolution used to simulate the secondary streamer are summarized in Table 2. We varied only one parameter in our simulations, E/N_{sec_max}, in the range 60 – 135 Td. The goal was to observe the typical increase of the $N_2(C)$ density during the secondary streamer phase (Fig. 8).

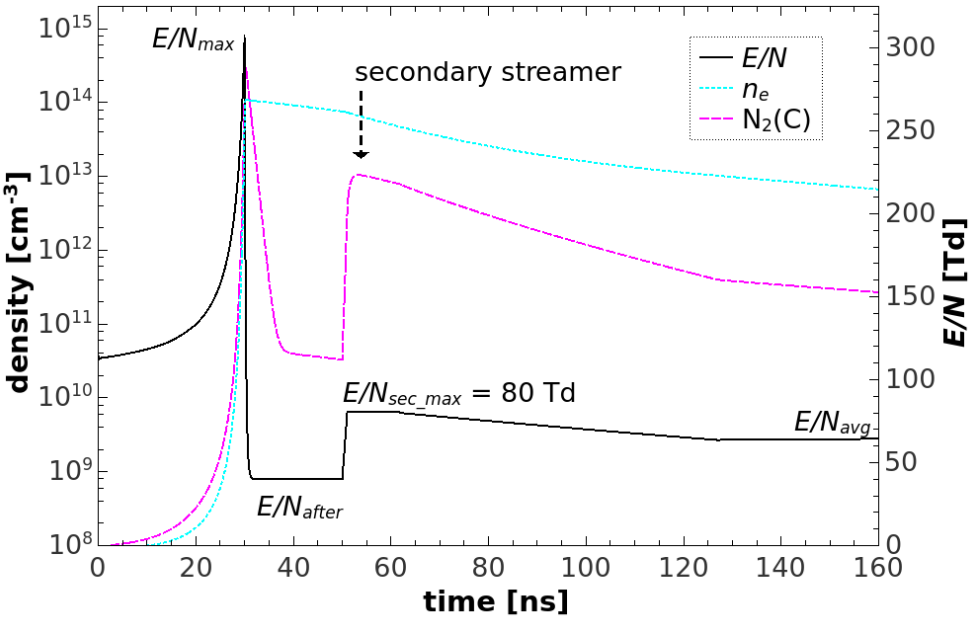

Fig. 7 – Temporal evolution of *E/N* simulating the primary and the secondary streamer near the anode, and calculated densities of $N_2(C)$ and electrons, E/N_{sec_max} = 80 Td, other primary and secondary streamer parameters are set according to Table 1 (column 3) and Table 2, respectively.

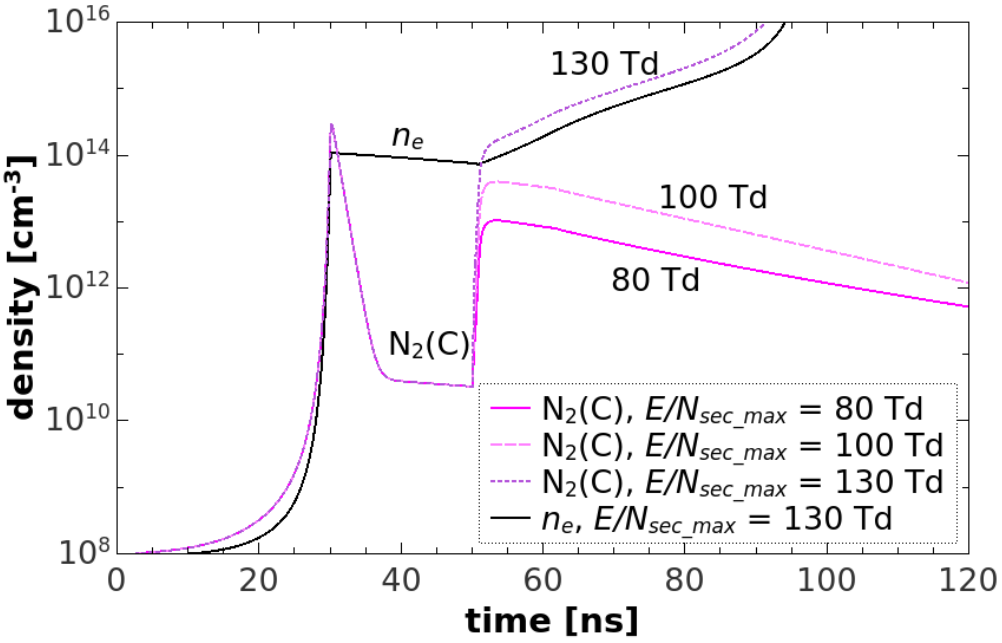

Fig. 8 – Temporal evolution of $N_2(C)$ density for different E/N_{sec_max} values, and electron density for E/N_{sec_max} = 130 Td only.

We observed that the *E/N* increase from E/N_{after} to E/N_{sec_max} leads to the appearance of the secondary peak in $N_2(C)$ density and this peak increases with increasing E/N_{sec_max}. According to the experimental data (Fig. 4), the $N_2(C)$ density during the secondary streamer should be ~2-3 times higher than during

the primary streamer. However, we were not able to reproduce this observation for E/N_{sec_max} below 130 Td, and the simulation with E/N_{sec_max} = 130 Td already indicates breakdown during the secondary streamer phase. This is not in agreement with experimental results showing the disappearance of the secondary streamer, and much later spark formation.

We assume that the only possible solution of this problem is the decrease of E/N_{max} during the primary streamer phase. This should decrease the density of $N_2(C)$ during the primary streamer, due to the lower n_e. The decrease of n_e during the primary streamer must be compensated by its increase during the secondary streamer phase. We therefore performed a set of calculations with E/N_{max} below 306 Td, and E/N_{sec_max} above 120 Td (in order to increase n_e). The goal was to achieve the maximum $n_e \approx 10^{14}$ cm^{-3} during the secondary streamer phase, with the ratio of $N_2(C)$ densities during the secondary and primary streamer to be ~2-3. We succeeded to achieve it for example for E/N_{max} = 292 Td and E/N_{sec_max} = 133 Td (Fig. 9). Other primary and secondary streamer parameters were as given in Table 1 (column 4) and Table 2, respectively. We also used these parameters for further calculations aiming to asses the role of the secondary streamer in plasma induced chemistry.

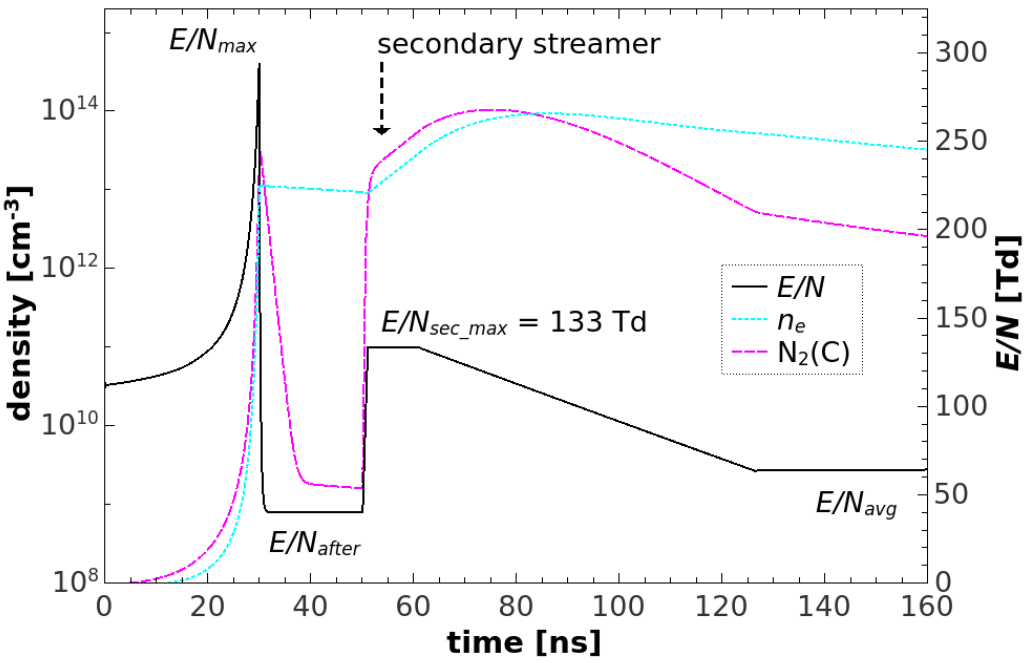

Fig. 9 - Temporal evolution of E/N simulating the primary and the secondary streamer near the anode, and calculated densities of $N_2(C)$ and electrons, E/N_{sec_max} = 133 Td, other primary and secondary streamer parameters according to Table 1 (column 4) and Table 2, respectively.

4.3 Influence of secondary streamer on plasma induced chemistry

In order to estimate the role of the secondary streamer on plasma induced chemistry, we will now compare two different conditions. First, the "strong" primary streamer (E/N_{max} = 306 Td) with no secondary streamer. Next, the "weak" primary streamer (E/N_{max} = 292 Td) followed by the secondary streamer (E/N_{sec_max} = 133 Td). Almost identical maximum $n_e \approx 10^{14}$ cm^{-3} was achieved in both simulations (Fig. 10). However, the duration of the secondary streamer is much longer compared to the primary streamer. Thus, despite the lower maximum E/N, the production of almost all studied RONS is much higher in the simulation with the secondary streamer. For illustration, Fig. 10 compares the temporal evolution of NO. The same is true for O, N and O_3. The only exception was NO_2, where the density decreased from the initial concentration ~10 ppm in both simulations.

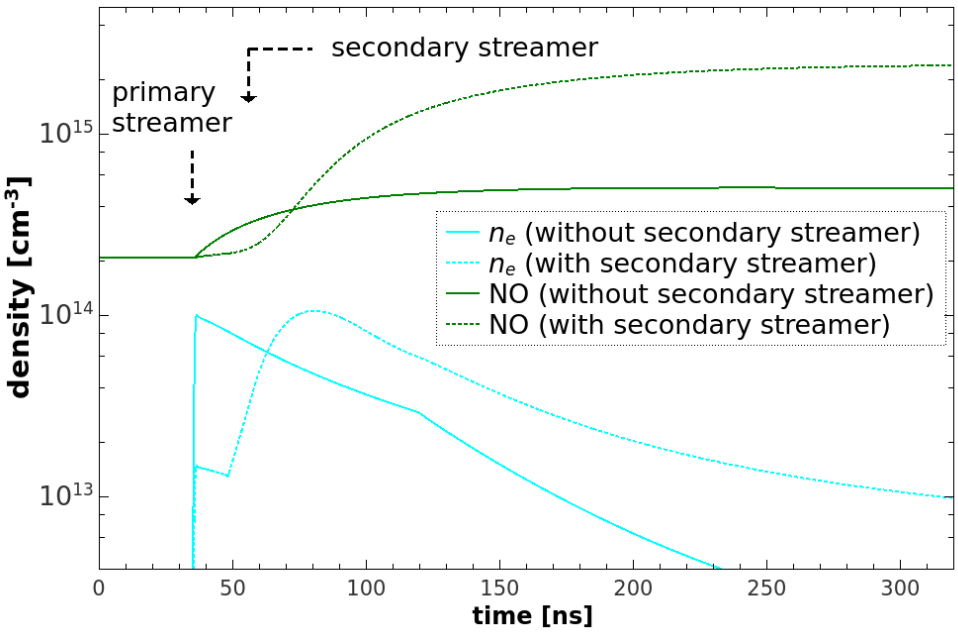

Fig. 10 – Temporal evolution of NO and electron densities in simulations with and without the secondary streamer.

It is interesting that 300 ns after the beginning of the simulations, the NO density is almost 1 order of magnitude higher with the secondary streamer then with "strong" primary streamer only (Fig. 10). However, we suppose that this finding does not explain dominant production of NO_x and almost no O_3 in the TS discharge. Figure 11 shows that the dominant product of the secondary streamer chemistry is O and its density is approximately 2 orders of magnitude higher than density of N. This indicates that in the cold atmospheric pressure conditions, the dominant final stable product should be the

ozone. To verify this hypothesis, we repeated a long time scale simulation without the spark phase after the secondary streamer, with a constant gas temperature (350 K) and gradual decrease of *E/N* after the secondary streamer down to 1.5 Td within 1 μs.

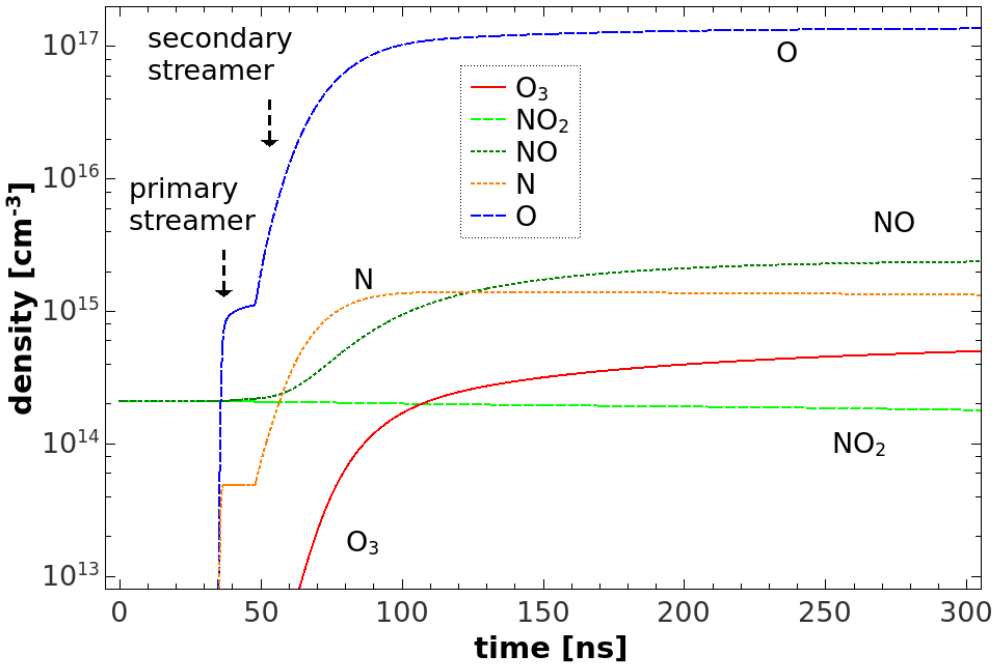

Fig. 11 – Calculated temporal evolution of selected RONS concentration in simulation with both primary (E/N_{max} = 292 Td) and secondary streamer (E/N_{sec_max} = 133 Td), short time scale.

We observed the same trends in the temporal evolution of the RONS as shown in Fig. 6. Again, the major product was ozone and NO was gradually converted to NO_2 (Fig. 12). Only the final densities of O_3 and NO_2 were almost by 1 order of magnitude higher than those obtained by the simulation without the secondary streamer (Fig. 6), and the conversion of NO to NO_2 was much faster. This conversion proceeds dominantly via two reactions:

$$NO + O_3 \rightarrow NO_2 + O_2, \quad (8a)$$

$$O + NO + N_2 \rightarrow NO_2 + O_2. \quad (8b)$$

Higher densities of both O_3 and O can thus explain faster NO to NO_2 conversion. In summary, the secondary streamer accelerates the overall chemistry, but only the spark phase can explain why the TS generates preferentially NO_x and O_3 was not experimentally detected. The spark phase simulations will be performed in near future to complete the chemistry kinetics of the entire TS repetitive cycle

and understand the overall final products that determine the antibacterial and other bio-relevant effects of the TS discharge.

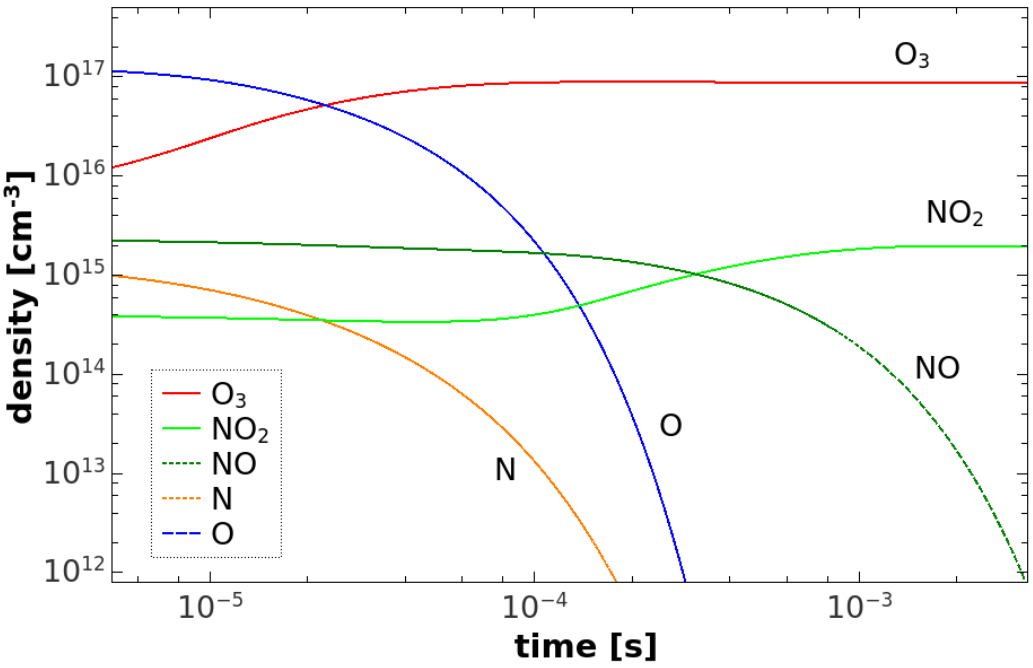

Fig. 12 – Temporal evolution of electrons and selected RONS densities on long time scale, simulating both primary and secondary streamer, input parameters as in Table 1 (column 4) and in Table 2, respectively.

5. Conclusions

The 0-D model based on ZDPlasKin module was successfully used to model plasma induced chemistry in the transient events propagating in space, such as primary and secondary streamers. The plasma chemistry and the efficiency of reactive species generation depends mainly on the reduced electric field strength *E/N*. Here we present temporal evolution of *E/N(t)* suitable to describe the initial phases of the transient spark discharge: the primary and the secondary streamers. The used *E/N(t)* was constructed based on experimental results and literature.

We focused on the secondary streamer and production of selected RONS playing important roles in biomedical effects of electrical discharges in air: O, N, NO, NO_2 and O_3. The secondary streamer results from the non-homogeneous axial distribution of plasma conductivity in the discharge channel created by the primary streamer. This results in non-homogeneous axial distribution of *E/N* that is

enhanced near the anode. By fitting the experimentally observed N_2 (C) 2nd positive system emission profiles we found out that the relatively high peak *E/N*, at least 120 Td, during the secondary streamer should be achieved. During the primary streamer the field is higher, but the duration of the secondary streamer is longer and higher electron density is achieved. For this reason, the secondary streamer strongly influences the density of produced reactive species. The density of NO is higher than the density of O_3 shortly after the secondary streamer. However the density of atomic oxygen is even higher and it strongly exceeds density of atomic nitrogen. When we simulated a hypothetical situation with primary and secondary streamer phases but no spark phase, the final dominant product was ozone.

In transient spark, however, the experimental data shows that NO and NO_2 are dominant products and there is no ozone. We assume that this results from the enhancement of atomic N generation and gas heating during the spark phase. We are planning further development of our kinetic model to be able to reliably simulate the spark phase of the TS discharge to prove this hypothesis and find better correlation with experiments.

Acknowledgement

This work was supported by Slovak Research and Development Agency APVV-0134-12, and Slovak Grant Agency VEGA 1/0419/18.

Appendix 1 – Parameters used to simulate the primary streamer

The formula describing the temporal evolution of the reduced electric field strength (*E/N*) during the primary streamer includes these adjustable input parameters: E/N_{before}, E/N_{max}, E/N_{after}, t_H, and l_t. The initial density of electrons $n_e(0)$, gas temperature ($T_g(0)$) and gas composition play also certain roles in chemical modeling. We performed our simulations in "synthetic dry air" with molar fraction of N_2 (χ_{N2}) and O_2 (χ_{O2}) being 0.8 and 0.2, respectively. Since the repetition rate of TS pulses is relatively high (~kHz), the gas composition between the electrodes is influenced by the previous TS pulses. However, the NO and NO_2 nitrogen oxides were the only significant stable gas phase products

measured experimentally, we thus included among the input parameters only the initial molar fraction of NO and NO_2.

Here we summarize why we used specific values of all these parameters and we will discuss their influence on the calculated electron density.

E/N_{before} – initial value of E/N:

The average E/N in the gap shortly before the primary streamer is around 60-70 Td. In the point-to-plane geometry the field is not homogeneous, and the E/N near the anode shortly before the beginning of the primary streamer propagation should be around 120 Td so that the ionization frequency exceeds the attachment frequency. For this reason we varied E/N_{before} in the range 60-120 Td. The final value of E/N_{before} = 100 Td most commonly used in our simulations, can be regarded as the typical value approximately 1-2 mm below the anode, where the field is slightly weaker than at the anode, but still higher than the average. Moreover, we found out that with E/N_{before} = 100 Td, the influence of the parameter t_H on our simulations is eliminated. The t_H describes the delay between the beginning of the simulation and the moment when the maximum E/N is achieved (the moment when the streamer's head virtually reaches the point in space where we study the chemical changes). With E/N_{before} < 100 Td, the electron density decreases from $n_e(0)$ down to certain minimal value n_e^{min} before it starts to grow again due to the increasing E/N. The electron density shortly before the streamer's head strongly influences the peak electron density during the primary streamer. With E/N_{before} < 100 Td, we would have to take into account n_e^{min} that depends on t_H and $n_e(0)$. For E/N_{before} = 100 Td, the electron density does not change significantly from $n_e(0)$ for at least 40 ns, i.e. $n_e^{min} \approx n_e(0)$, and thus the parameter t_H plays no role.

E/N_{max} – peak E/N value in the streamer's head:

The value of E/N_{max} used in our simulations (200-350 Td) is in agreement with our experimental findings [31]. The experimentally measured E/N_{max} increased from ~200±50 up to 300±50 Td during the streamer propagation towards the cathode,. In our simulations, we adjusted the E/N_{max} in order to achieve the desired peak electron density according to the experimental results. We could achieve a wide range of electron densities by tuning the E/N_{max} within the range of experimental uncertainty. The E/N_{max} is not the only parameter determining the peak electron density, it also strongly depends on $n_e(0)$. The desired peak electron density can be thus achieved by various pairs of E/N_{max} and $n_e(0)$ values. However, further evolution of the electron density after the primary streamer does not depend

on the chosen pair. The E/N drops quickly from E/N_{max} to much lower E/N_{after} after the primary streamer, the generation of electrons stops and processes decreasing n_e dominate.

E/N_{after} – reduced field behind the streamer's head:

The average E/N in our gap shortly before the streamer is around 60-70 Td and the field behind the streamer's head E/N_{after} should be slightly lower compared to this average value. We thus tested E/N_{after} in the range 40-70 Td. Within this range the field is very low for an effective ionization and has no significant influence on the electron density evolution. Moreover, the period with E/N = E/N_{after} is very short. So, finally we decided to use E/N_{after}=40 Td. This enabled us to test the E/N in the secondary streamer from 60 Td.

l_t – primary streamer characteristic time:

Roughly speaking, the time constant l_t characterizes how fast is the increase of E/N to E/N_{max}. The propagation of the primary streamer is quite fast (Fig. 3). It takes up to ~5 ns to propagate from the anode to a virtual point 2 mm below. This limits the possible value of l_t to range 1-3 ns. We decided to use 2 ns in our simulations.

$n_e(0)$ – initial electron density:

The initial electron density plays quite important role with respect to the achieved peak electron density during the primary streamer. Though, the peak electron density is more sensitive on E/N_{max} than on $n_e(0)$. We have no direct experimental data to determine $n_e(0)$, we thus tested a wide range of possible values (10^3 – 10^{10} cm^{-3}) relying on Meek's criterion. The electron avalanche that enables formation of the streamer must generate enough charged particles (~10^8) for distortion of the external applied field. If this charge is localized at the anode in a volume of 1 mm^3, the resulting average electron density in this volume is in order of 10^{11} cm^{-3}. We assumed that two mm below the tip of the anode, the electron density is certainly lower, in order of 10^{10} cm^{-3} or lower. We finally decided to use $n_e(0)$ = 10^8 cm^{-3}, but as we show in Fig. 5, the value of $n_e(0)$ does not influence the evolution of the electron density after the primary streamer at all. It just influences the value of E/N_{max} which we must use to obtain the desired peak electron density; lower $n_e(0)$ means higher E/N_{max}. While using $n_e(0)$ = 10^8 cm^{-3}, the required E/N_{max} is in good agreement with experimentally observed values.

$T_g(0)$ – gas temperature:

Due to the repetitive character of the TS discharge, with the repetition rate in order of kHz, the pre-heating of the treated gas by precedent pulses occurs. Based on spectroscopic data [41], the

temperature at the beginning of the primary streamer ($T_g(0)$) is elevated to ~350 K at TS repetition frequency ~1 kHz. We used this value in our simulations. Comparison with simulations where $T_g(0)$ = 300 K revealed that there is negligible influence on the peak electron density, it just slightly influences the rate of electron density decay afterwards. Lower temperature means higher density of O_2, i.e. slightly higher rate of electron attachment reactions.

χ_{NO} and χ_{NO2} – initial molar fractions of NO and NO_2:

The analysis of air treated by TS discharge [26] revealed that NO and NO_2 were major stable products. Their detected densities highly exceeded 100 ppm, i.e. molar fraction 10^{-4}. However, these densities were measured downstream long after the treatment and the steady-state concentrations of these species in the gap between the electrodes can be theoretically much higher, but also much lower if we assume that most NO_x molecules are produced downstream from N and O atoms generated during the spark pulse. We therefore tested quite wide range of χ_{NO} and χ_{NO2} – from 0 to 10^{-4}. Here we present results for $\chi_{NO} = \chi_{NO2} = 10^{-5}$. Within the studied range, χ_{NO} and χ_{NO2} have no significant influence on electron density during the primary and the secondary streamer. For example, if $\chi_{NO} = \chi_{NO2} = 0$, the E/N_{max} must be only by about 1 Td higher to achieve the same peak electron density compared to $\chi_{NO} = \chi_{NO2} = 10^{-5}$. Moreover, χ_{NO} and χ_{NO2} within the studied range have also no significant influence on calculated final densities of NO and NO_2 long after the secondary streamer.

Using molar fraction 10^{-5} instead of 0 enabled us to observe both production and sink mechanisms of NO_x during the TS streamer phase.

References

[1] Janda M et al. (2011) Plasma Sources Sci Technol 20:035015

[2] Janda M et al. (2014) Plasma Sources Sci Technol 23:065016

[3] Janda M et al. (2012) Stabilization of a lean methane-air flame using transient spark discharge. In: Janowski T et al. (ed) International symposium on high pressure low temperature plasma chemistry HAKONE XIII (Kazimierz Dolny, Poland, 9-14 September), pp 185-189

[4] Walsh JL, Shi JJ, Kong MG (2006) Appl Phys Lett 89:161505

[5] Pancheshnyi SV et al. 2006 IEEE Trans Plasma Sci 34:2478-2487

[6] Pai D, Lacoste DA, Laux CO (2008) IEEE Trans Plasma Sci 36:974-975

[7] Hensel K et al. (2015) Biointerphases 10 :029515

[8] Hontanon E et al. (2013) J Nanopart Res15:1957

[9] Graves DB (2012) J Phys D Appl Phys 45:263001

[10] Lukeš P et al. (2014) Plasma Sources Sci Technol 23:015019

[11] Ying Li et al. (2017) Sci Rep 7:45781

[12] Ishaq M, Evans M, Ostrikov K (2014) Int J Cancer 134:1517

[13] Eliasson B, Hirth M, Kogelschatz U (1987) J Phys D Appl Phys 20:1421-1437

[14] Gordeyenya EA, Matveyev AA (1994) Plasma Sources Sci Technol 3:575-583

[15] Knizhnik AA et al. (1999) Doklady Akademii Nauk 365:336-339

[16] Rehbein N, Cooray V (2001) J Electrostat 51-52:333-339

[17] Rahman M, Cooray V (2003) Opt Laser Technol 35:543-546

[18] Kim T et al. (2010) Jpn J Appl Phys 49:126201

[19] Rahman M et al. (2011) J Electrostat 69:494-500

[20] Shank JL, Herper RH, Silliker JH (1962) Appl Microbiol 10:185-189

[21] Mancinelli RL, McKay CP (1983) Appl Environ Microbiol 46:198-202

[22] Carbone P et al. (2013) Device and method for gas sterilization. US Patent 2013/0230430A1

[23] Pavlovich MJ et al. (2014) J Phys D Appl Phys 47:505202

[24] Moiseev T et al. (2014) Plasma Sources Sci Technol 23:065033

[25] Hao XL et al. (2014) Plasma Process Polym 11:1044-1056

[26] Janda M. at al. (2016) Plasma Chem Plasma Process 36:767-781

[27] Van Gaens W, Bogaerts A (2014) Plasma Sources Sci Technol 23:035015

[28] Lu X et al. (2016) Phys Rep 630:1-84

[29] Jenista J (1999) J Phys D Appl Phys 32:2763-2776

[30] Barni R et al. (2005) J Appl Phys 97:073301

[31] Janda M et al. (2017) Plasma Sources Sci Technol 26:055010

[32] Janda M et al. (2017) J Phys D Appl. Phys 50:425207

[33] Morrow R, Lowke JJ (1997) J Phys D Appl Phys 30:614-27

[34] Kulikovsky AA (1998) IEEE Trans Plasma Sci 26:1339-46

[35] Marode E et al. (2009) Plasma Phys Control Fusion 51:124002

[36] Loeb LB (1965) Electrical Coronas: Their Basic Physical Mechanisms (Berkeley, CA: University of California Press)

[37] Bastien F, Marode E (1985) J Phys D Appl Phys 18:377

[38] Sigmond SR (1984) J Appl Phys 56:1355

[39] Ono R, Oda T (2007) J Phys D Appl Phys 40:176

[40] Dvonč L, Janda M (2015) IEEE Trans Plasma Phys 43:2562-2570

[41] Janda M et al. (2012) Plasma Sources Sci Technol 21:045006

[42] Gerling T et al. (2013) Plasma Sources Sci Technol 22:065012

[43] Pancheshnyi S et al. (2008) Computer Code ZDPlasKin, Univ. Toulouse, Toulouse, LAPLACE, CNRS-UPS-INP, France. [Online]. Available: https://www.zdplaskin.laplace.univ-tlse.fr

[44] Brown PN, Byrne GD, and Hindmarsh AC 1989, VODE: A variable-coefficient ODE solver, SIAM J. Sci. Stat. Comput. 10 1038–1051

[45] kinet_N2_O2_v1.03 (2015) [Online]. Available: http://www.zdplaskin.laplace.univ-tlse.fr/wp-content/uploads/2015/08/kinet_N2_O2_v1.03.inp

[46] Capitelli M et al. (2000) Plasma Kinetics in Atmospheric Gases (Springer Series on Atomic, Optical, and Plasma Physics). New York, NY, USA: Springer-Verlag.

[47] Flitti A, Pancheshnyi S (2009) Eur Phys J Appl Phys 45:21001

[48] Hagelaar GJM and Pitchford LC 2005 Plasma Sources Sci. Technol. 14, 722-733

[49] Pancheshnyi S et al. (2012) Chem Phys 398:148

[50] Phelps Database. (retrieved on Mar. 13, 2014) [Online]. Available: (www.lxcat.net/Phelps) (http://jilawww.colorado.edu/~avp/)

[51] Phelps AV, Pitchford LC (1985) Phys Rev A 31:2932-2949

[52] Morgan Database. (retrieved on May 26, 2014). [Online]. Available: http://www.lxcat.net/Morgan

[53] Hayashi Database. (retrieved on May 26, 2014). [Online]. Available: http://www.lxcat.net/Hayashi

[54] QUANTEMOL database. (retrieved on Feb. 15, 2018). [Online]. Available: (www.lxcat.net/QUANTEMOL) (http://quantemol.com)

[55] Kulikovsky AA (1997) J Phys D Appl Phys 30:441-450

[56] Kacem S et al. (2012) J Comput Phys 231:251-261

[57] Bourdon A, Bonaventura Z, Celestin S (2010) Plasma Sources Sci Technol 19:034012

[58] Naidis GV (2009) Phys. Rev. E 79:057401

[59] Bonaventura Z et al. (2011) Plasma Sources Sci Technol 20:035012

[60] Hoder T et al. (2015) J Appl Phys 117:073302